

Nano-Scale Hydroxyapatite Coating on Macroscopic Silica Fiber Using Carbon Nanofibers as Templates

Qiang Wu,[1] Hitoshi Ogihara,[1] Hisaichiro Uchida,[2] Masahiro Sadakane,*[1] Yoshinobu Nodasaka,[3] and Wataru Ueda[1]

[1]Catalysis Research Center, Hokkaido University, N21, W10, Sapporo 001-0021

[2]Development Department, Tosco Co., LTD., 2-13-67 Shiro-machi, Mihara 723-0014

[3]Graduate School of Dental Medicine, Hokkaido University, N13, W7, Sapporo 060-8586

Received August 3, 2007; E-mail: sadakane@cat.hokudai.ac.jp

Starting from $Ca(NO_3)_2$–H_3PO_4–methanol precursor mixtures and using carbon nanofibers (CNFs) as templates, we have successfully coated nano-scale hydroxyapatite (HAp) layers on macroscopic silica fiber (diameter ca. 5 μm) surfaces. Under controlled experimental conditions, CNFs can be formed on silica fiber with variable yield, layer thickness, and diameters, and thus can be further used as different templates for HAp coating. XRD, FE-SEM, and cross-sectional TEM experimental results provided clear evidence that CNFs can act as effective templates for uniform nano-scale HAp coating on silica fiber. It turned out that heat-treatment at 923 K for 5 h is sufficient for complete removal of the CNFs templates and crystallization of the resulting nano-scale HAp. It was shown that the resulting HAp layer thickness was ca. 2–4 μm, the average crystallite size was ca. 20–40 nm, and the specific surface area was ca. 50–65 $m^2\,g^{-1}$. In addition, it was clearly demonstrated that the average layer thickness and amount of HAp was controlled by the layer thickness of CNFs. Therefore, the coating mode of HAp could be reliably controlled through the selection of different kinds of CNFs templates.

Hydroxyapatite (HAp), which is well known as the main mineral component of bones and teeth, has been extensively studied and applied in a variety of fields due to its excellent bioactivity, biocompatibility, osteoconductivity, ion-exchange ability, adsorption capacity, and catalytic ability.[1–12] In recent years, significant research efforts have been devoted to the development of HAp coating on other substrates so as to improve its potential for practical applications. Various techniques, such as electrophoretic deposition,[13] hot isostatic pressing,[14] biomimetic processes,[15] plasma spraying,[16] and alternate soaking processes[17] have been employed to produce an HAp layer on the substrate. Electrophoretic deposition (EPD) is an attractive method for HAp synthesis, however, it is difficult to control the applied voltages and deposition time needed to obtain uniform HAp. Hot isostatic pressing (HIP) of HAp coating onto the substrate needs to be carried out under considerably high temperature and pressure. Biomimetic processing for HAp coating can be realized by immersing the substrate into simulated body fluid (SBF) solution for a very long time. Plasma spraying allows large amounts of HAp coating on the substrate, but the long-term stability of these coatings is still a challenging problem. Furthermore, this procedure needs to be performed under very high pressure. Alternate soaking processes can also bring about mass HAp coating on the substrate after many soaking cycles. Up to now, uniform HAp coating on any substrate is still a challenging issue.

Recently, we have demonstrated that carbon nanofibers (CNFs) are promising and effective templates for the formation of nano-scale materials.[18,19] Notably, CNFs can be easily synthesized under mild reaction conditions by the decomposition of hydrocarbons over metal catalysts such as nickel, cobalt, iron, and their alloys.[20] Also, the structure of CNFs can be tuned by changing the synthesis parameters (such as reaction temperature, carbon source, and metal catalyst used). In addition, CNFs can be easily removed by oxidation or hydrogenation due to their high reactivity with O_2, CO_2, and H_2.[21] These merits make them suitable for acting as promising templates for the synthesis of new tubular materials.

In a very recent communication,[22] we reported a facile method to uniformly coat silica fiber with nano-scale fibrous $LaMnO_3$ by using CNFs as templates. It seemed that the uniform formation of CNFs on silica fiber is a prerequisite for the subsequent uniform formation of $LaMnO_3$ but this hypothesis needs more experimental evidence to support it. Furthermore, how the CNFs performed as effective templates for the formation of $LaMnO_3$ on silica fiber still is not fully understood. In this paper, we extend this promising template method to the fabrication of nano-scale HAp on silica fiber. Structural characterization of both CNF-coated silica fiber and HAp-coated silica fiber is described in detail. Particular attention is given to the influence of different kinds of CNF templates on HAp coating via the template route. It is expected that such nano-scale HAp with direct macroscopic shapes hold promise as highly functionalized materials. Despite the above obvious potential, to the best of our knowledge, this is the first report on the coating of nano-scale HAp on macroscopic silica fiber through a single methanol solution of $Ca(NO_3)_2$–H_3PO_4. Compared with other applied techniques used for HAp coating, the CNF template method is a facile and effective process.

Published on the web March 13, 2008; doi:10.1246/bcsj.81.380

Experimental

Materials. $Ni(NO_3)_2 \cdot 6H_2O$, $Ca(NO_3)_2 \cdot 4H_2O$, H_3PO_4, acetone, and methanol were used as received without further purification. Silica fiber (Tosoh, Japan, diameter ca. 5 μm) was adopted as a substrate to synthesize CNF templates. Commercial HAp (HAP-100) and commercial Tricalcium Phosphate (β-TCP) (Taihei Sangyo, Japan) were selected for comparative study.

Preparation of CNFs Templates. CNF templates were synthesized by the decomposition of methane over NiO/silica fiber catalyst. First, NiO/silica fiber catalyst (ca. 1 wt % as NiO) was prepared by impregnating silica fiber (ca. 0.2 g) with 0.3 M $Ni(NO_3)_2$ acetone solution at room temperature. Excess solution was removed by vacuum filtration. Afterwards, the resulting impregnated sample was calcined in air at 573 K for 1 h to obtain the NiO/silica fiber catalyst. Finally, the decomposition of methane (flow rate = 20 mL min^{-1}) was performed over the catalyst from 773 to 873 K for 2 h with a conventional gas-flow system at atmosphere pressure. Prior reduction of the catalyst under hydrogen was not necessary, because the nickel oxide form is easily reduced in the reaction by methane.

HAp Coating on Silica Fiber Using CNFs as Templates. A typical synthetic procedure is as follows: CNF templates were first placed into a suction filtration unit. Then, a precursor solution consisting of 2.0 M $Ca(NO_3)_2$ and 1.2 M H_3PO_4 in methanol (the ratio of Ca/P is 1.67) was dropped into the CNF templates. Excess solution was removed by vacuum filtration. After that, the resulting samples were dried in air at 393 K (30 min) and then at 573 K (30 min). Finally, the templates were removed by calcination in air at given temperatures for 5 h to obtain the desired samples.

Characterizations. Field emission scanning electron microscopy (FE-SEM) measurements were carried out using a JSM-7400F (JEOL) instrument. Energy dispersive spectroscopy (EDS) experiments were done using a JSM-6360 LA (JEOL) scanning electron microscope coupled with a JED-2300 (JEOL) EDS unit. Quantitative analysis was performed by ZAF method. Transmission electron microscopy (TEM) was conducted on an H-800 (HITACHI) or a JEM-2000 FX (JEOL) instrument operated at 200 kV. Before analysis, samples were put into ethanol and subsequently sonicated for 3 min. A few drops of the resulting suspension were then placed on perforated carbon film on a copper grid. Cross-sectional specimens for TEM measurements were obtained as follows: samples were first embedded in epoxy resin after polymerization of the matrix by heating at 333 K for 48 h, the samples were then cut in ca. 80 nm thick sections on an ultramicrotome. X-ray diffraction (XRD) measurements were recorded on a RINT Ultima + (Rigaku) diffractometer with Cu Kα radiation (tube voltage: 40 kV, tube current: 20 mA). The diffraction line widths were obtained after subtraction of the instrumental width determined by the linewidth of a silicon powder sample, and crystallite sizes were calculated from the width of the (002) line using the Scherrer equation. Raman spectra of solid-state samples were measured with an NRS-1000 (JASCO) FT-Raman spectrometer. Temperature-programmed oxidation (TPO) experiments were carried out via a home-made instrument, connected to an M-QA100S (ANELNA) quadrupole mass spectrometer for online gas detection. The m/z ratios of 18 (H_2O), 28 (CO), 32 (O_2), and 44 (CO_2) were monitored. The temperature was programmed from 303 to 1073 K at a heating rate of 10 K min^{-1}. Thermogravimetry and differential thermal analysis (TG-DTA) were carried out on a Thermo Plus TG 8120 (Rigaku) instrument at a heating rate of 10 K min^{-1} and a temperature region from room temperature to 1073 K. Elemental analyses were performed by the center for Instrumental Analysis at Hokkaido University. Brunauer–Emmett–Teller (BET) specific surface areas were estimated by using an AUTOSORB-3 (YUASA IONICS) sorption analyzer after degassing at 473 K for 2 h.

Results and Discussion

Characterization of CNFs Templates. The typical morphology of the pure silica fiber is straight with a relatively smooth surface, with a diameter of ca. 5 μm (insets of Fig. 1a). Figures 1a–1f show the FE-SEM images of CNFs formed by methane decomposition over NiO/silica fiber catalyst at different synthesis temperatures for 2 h. After decomposition of methane, the value of carbon deposition was calculated: Carbon deposition (%) = $100 \times W_{\text{deposited carbon}}/W_{\text{Ni}}$, where $W_{\text{deposited carbon}}$ is the weight of carbon deposited on the silica fiber, and W_{Ni} is the weight of Ni on the fiber. The CNFs synthesized at 773, 823, and 873 K were designated as CNFs-773, CNFs-823, and CNFs-873, respectively. For the obtained CNFs, it was found that the carbon deposition increased with the synthesis temperature, and the corresponding values were calculated to be 6360%, 12980%, and 23160% for CNFs-773, CNFs-823, and CNFs-873, respectively (Table 1). These values are comparative to a value of Ni on SiO_2 (Kieselgel).[23] As can be seen from the FE-SEM images (Figs. 1a, 1c, and 1e), the CNF layer completely and uniformly covered the surface of the fiber. The average layer thickness of the obtained CNFs could be calculated based on FE-SEM analysis, and the corresponding value was ca. 3 μm for CNFs-773, 5 μm for CNFs-823, and 7 μm for CNFs-873 (Table 1). According to the FE-SEM images in Figs. 1b, 1d, and 1f, it was shown that CNFs were entangled and their diameters varied from 20 to 50, 30 to 80, and 40 to 90 nm for CNFs-773, CNFs-823, and CNFs-873, respectively. This means that the layer thickness and diameter of CNFs can be controlled by the synthesis temperature. A typical cross-sectional TEM image of CNFs-823 (Fig. 1g) confirmed that CNFs were grown on the outer surface of silica fiber, and the CNF layer thickness was in the range of 5–6 μm, which agrees well with the FE-SEM results. It should be pointed out that the absence of silica fiber inside the CNFs layer (white hole) in the cross cross-sectional TEM images was due to the breakage of physically hard fiber through cutting by an ultramicrotome. Black rods in the white hole are broken silica fiber pieces. In addition, the TEM image of CNFs-823 illustrates that the diameters of CNFs were distributed from 30 to 80 nm (Fig. 1h), consistent with the FE-SEM result (Fig. 1d). From the insets of Fig. 1h, it was confirmed that a nickel metal particle was present at the tip of the CNFs, indicating that CNF growth follows common tip-growing mode. The specific surface areas of the obtained CNFs ranged from 80 to 90 $m^2\ g^{-1}$ (Table 1).

TG curves of the obtained CNFs indicated only one weight loss stage for each case (Fig. S1, Supporting Information), and the half combustion temperatures were ca. 850, 880, and 890 K for CNFs-773, CNFs-823, and CNFs-873, respectively, which are common combustion temperature ranges for CNFs.

XRD measurements reveal that the predominant peak responsible for the diffraction of the graphite (002) plane was

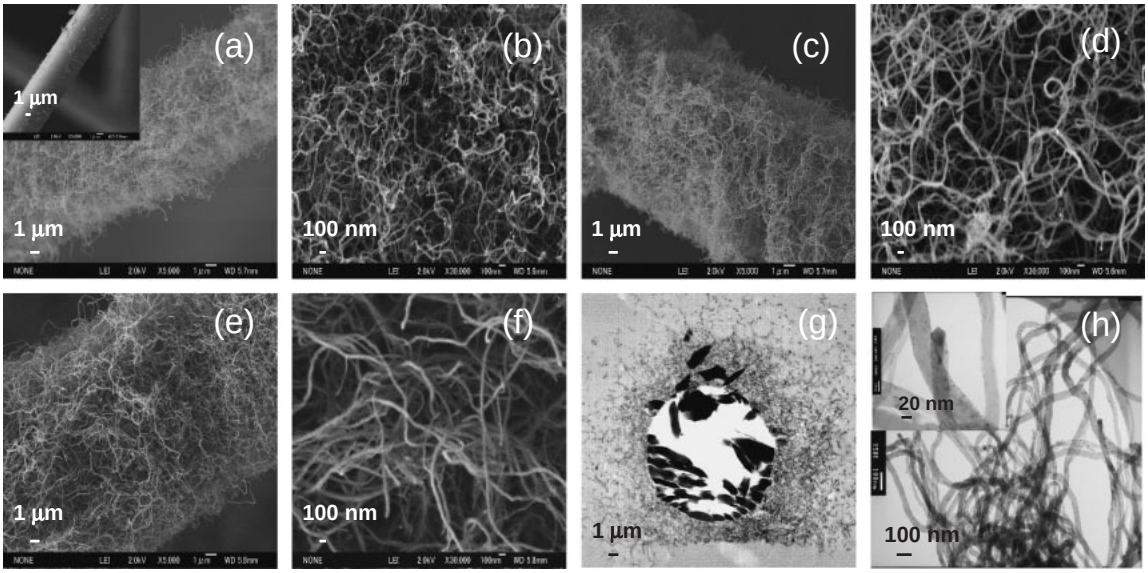

Fig. 1. (a, b) FE-SEM images of CNFs synthesized at 773 K, inset shows FE-SEM image of pure silica fiber, (c, d) CNFs synthesized at 823 K, (e, f) CNFs synthesized at 873 K, (g) Cross-sectional TEM image of CNFs synthesized at 823 K, the absence of silica fiber inside the CNF layer (white hole) in the cross cross-sectional TEM images was due to the breakage of physically hard silica fiber through cutting by an ultramicrotome. Black rods in the white hole are broken silica fiber pieces. (h) TEM images of CNFs synthesized at 823 K.

Table 1. Physical Properties of CNFs and HAps on Silica Fiber

	CNFs					HAp[b)]			
Samples[a)]	Carbon deposition on silica fiber/%[c)]	Carbon deposition based on Ni /%[d)]	Average layer thickness /μm	Diameters /nm	Specific surface areas /$m^2\ g^{-1}$	Amount of coated HAp[e)] /%	Average layer thickness /μm	Crystallite sizes[f)]/nm	Specific surface areas /$m^2\ g^{-1}$
CNFs-773	50	6360	3	20–50	87	33	2	22	58
CNFs-823	102	12980	5	30–80	84	44	3	25	61
CNFs-873	180	23160	7	40–90	80	78	4	31	53

a) The CNFs synthesized at 773, 823, and 873 K are denoted as CNFs-773, CNFs-823, and CNFs-873, respectively. b) HAp was produced by a calcination at 923 K. c) Carbon deposition (%) $= 100 \times W_{\text{deposited carbon}}/W_{\text{silica fiber}}$, where $W_{\text{deposited carbon}}$ is the weight of carbon deposited on the silica fiber, and $W_{\text{silica fiber}}$ is the weight of silica fiber. d) Carbon deposition (%) $= 100 \times W_{\text{deposited carbon}}/W_{\text{Ni}}$, where $W_{\text{deposited carbon}}$ is the weight of carbon deposited on the silica fiber, and W_{Ni} is the weight of Ni on the silica fiber. e) Amount of coated HAp (%) $= 100 \times W_{\text{coated HAp}}/W_{\text{silica fiber}}$, where $W_{\text{coated HAp}}$ is the weight of coated HAp on the silica fiber, and $W_{\text{silica fiber}}$ is the weight of the silica fiber. f) Crystallite sizes were estimated from the width of the (002) line using the Scherrer equation.

pretty clear for all the obtained CNFs (Fig. S2, Supporting Information), indicating that the CNFs were highly graphitized. It was found that the interplanar distance $d(002)$ values of the CNFs were 0.340, 0.338, and 0.337 nm for CNFs-773, CNFs-823, and CNFs-873, respectively, which are slightly higher than that of the ideal graphite (0.335 nm).

Moreover, based on the representative Raman spectra characterization (Fig. S3, Supporting Information), the ratio of the intensity of D band to G band (I_D/I_G) was calculated to be 1.83 for CNFs-773, 1.77 for CNFs-823, and 1.47 for CNFs-873. Similar I_D/I_G values were reported by Takenaka et al.[23] These results indicate that the CNFs grown on silica fiber have similar properties to CNFs produced by the decomposition of methane on NiO/silica.

Based on the above results, we can conclude that different kinds of CNFs can be formed by controlling the synthesis temperature during the decomposition of methane on NiO/silica fiber. In the present study, CNFs-823 was selected as the typical template for further investigation of HAp coating, and eventually CNFs-773 and CNFs-873 were also used to investigate the influence of different kinds of templates on the subsequent HAp coating.

HAp Coating on Silica Fiber with and without CNF Template. HAp coating on silica fiber with and without CNF template was first checked by FE-SEM measurements. Figure 2a shows the FE-SEM image of the obtained HAp coating using CNFs-823 as templates and calcinated at 923 K for 5 h. It is apparent that using CNFs-823 as templates can readily promote large amounts of uniform HAp on silica fiber. The average HAp layer thickness was calculated to be ca. 3 μm, and the weight gain of HAp on the fiber (i.e. the weight of obtained HAp divided by the weight of the original silica fiber) was calculated to be ca. 44%. For comparison, pure silica fiber was also submitted to the same experiment. We observed that only traces of HAp were present on pure silica (Fig. 2b), and the weight gain of HAp was calculated to be only ca. 10%.

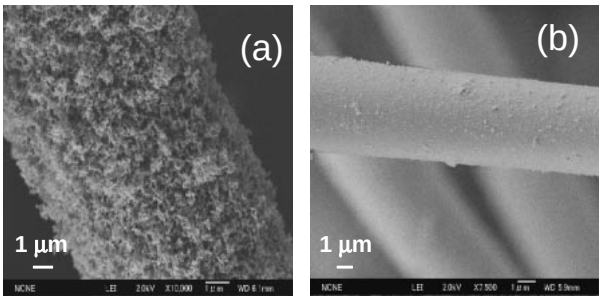

Fig. 2. (a) FE-SEM image of HAp coating on silica fiber using CNFs-823 as templates, (b) FE-SEM image of HAp coating on silica fiber without template.

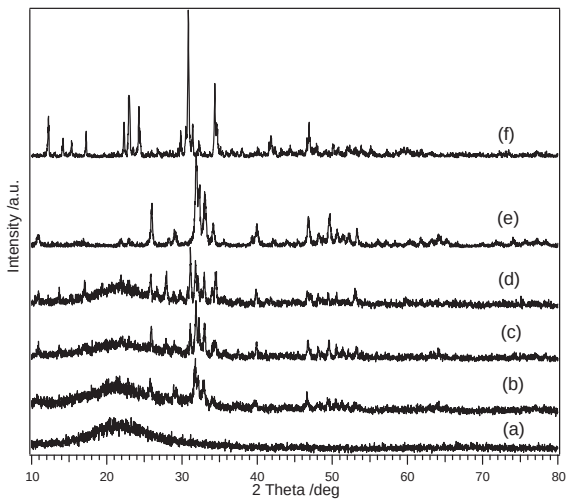

Fig. 3. XRD patterns of (a) pure silica fiber, (b) nano-scale HAp coating on silica fiber using CNFs-823 as templates calcinated at 923 K, (c) nano-scale HAp coating on silica fiber using CNFs-823 as templates calcinated at 1073 K, (d) nano-scale HAp coating on silica fiber using CNFs-823 as templates calcinated at 1273 K, (e) commercial HAp, and (f) commercial β-TCP.

The above results indicate that CNFs are indispensable for coating HAp on silica fiber. In addition, to get more detailed information, coating of HAp was also evident from the cross-sectional TEM measurements. The cross-sectional TEM image in Fig. S4 (Supporting Information) confirmed that HAp layer thickness varied from 2.5 to 3.5 μm, which was almost at the same level as calculated from FE-SEM results (Fig. 2a). The cross-sectional TEM image also shows that the shapes of HAp layers were similar to those of CNF layers on silica fiber (Fig. 1g). This strongly suggested that CNFs-823 worked as templates in HAp synthesis. Thus, we can conclude that CNFs-823 is a promising and effective template for coating HAp on silica fiber.

In order to be sure of the phase composition, the obtained HAp coating was further characterized by XRD measurements (Fig. 3b). For comparison, the XRD patterns of commercial HAp, β-TCP, and pure silica fiber calcinated at 923 K for 5 h were also recorded. Broad peaks of silica fiber were observed at $2\theta = 22.2^\circ$. It can be seen that XRD patterns show diffraction peaks in good agreement with the commercial HAp. In addition, the average crystallite size of HAp was estimated by Scherrer equation analyzing the half-band widths of the diffraction peaks at $2\theta = 25.8^\circ$ due to the HAp (002) plane, and the value was calculated to be 25 nm. The above XRD results again strongly confirmed that CNFs-823 is an effective template for coating nano-scale HAp on silica fiber.

Analysis of the Heating Process for HAp Coating on CNFs-823 Templates. It is well accepted that temperature control during the synthesis process is very important to the properties of the resulting HAp materials coating the substrate.[3] Thus, HAp coating on CNFs-823 templates and its thermal stability were studied by TG-DTA measurements. Figure S5 shows the TG-DTA curves of the precursor methanol solution (Ca/P ratio of 1.67) penetrated into a CNFs-823 template before calcination (only dried in air at 393 K for 30 min before TG-DTA measurements). TG curves show four main weight losses in the temperatures ranges of 310–360, 600–650, 700–820, and 980–1000 K. Accordingly, there appeared four endothermic or exothermic peaks in the DTA curves. The first endothermic peak corresponding to the first weight loss (ca. 9%) should be assigned to the evaporation of absorbed and chemisorbed water.[24] The second exothermic peak corresponding to the second weight loss (ca. 7%) probably originated from the reaction of CNFs-823 templates with nitrates. Since we can obtain proof in Fig. S6 (Supporting Information), it was shown that during the TPO process of HAp coating on CNFs-823 templates, NO (30), CO_2 (44), and CO (28) were observed in the product mixture in the 600–650 K region. Thus, it can be confirmed that these products came from the reaction of CNFs-823 templates with nitrates, while the strong and main broad exothermic peak in Fig. S5 corresponding to the third weight loss (ca. 23%) resulted from the removal of CNFs-823 during the calcination process. Based on the TG-DTA experiments, it can be concluded that the presence of $Ca(NO_3)_2$ and H_3PO_4 can facilitate the combustion of CNFs-823 templates, and the starting temperature of CNFs-823 combustion was decreased from ca. 760 to 670 K. In addition, the weak and small endothermic peak in Fig. S5 corresponding to the last weight loss (ca. 3%) is probably due to partial decomposition of the resulting HAp into β-TCP.[25,26] Through TG-DTA analysis, we can reach the conclusion that the optimal calcination temperature region for HAp formation via template method is approximately from 820 to 980 K, because in this temperature region, CNFs-823 can be fully removed by calcination in air and the resulting HAp was relatively thermally stable on silica fiber.

Role of CNFs for the Homogeneous Coating of HAp on Silica Fiber. During the impregnation stage, the precursor solution can rapidly diffuse into the whole layer of CNF on silica fiber by capillary force. In this period, CNFs act as a "sponge," it can supply some "reservation" room for the precursor solution, and the solution remains in the space during the following filtration process. Furthermore, we believe the surface of CNF was oxidized by nitrate to form functional groups (such as –COOH and –C=O). Such functional groups can serve as anchoring sites for Ca^{2+} ions, followed by the incorporation of PO_4^{3-} ions to form amorphous calcium phosphate derivatives which can be transformed to the desired HAp during the calcination. Further detailed investigation is underway in our laboratory.

Phase Composition and Morphology of the Obtained HAp on Silica Fiber at Different Calcination Temperatures Using CNFs-823 as Templates. Figure 3 shows the XRD patterns of the obtained nano-scale HAp on silica fiber obtained at different calcination temperatures using CNFs-823 as templates. The calcination time was kept at 5 h and the calcination temperatures were 923, 1073, and 1273 K. These temperatures were determined so as to confirm the phase identification of each sample, and to confirm the optimal calcination temperature based on the TG-DTA results. As can be seen from Fig. 3, the XRD patterns of the HAp on silica fiber obtained at different calcination temperatures (Figs. 3b–3d) correspond to the characteristic peaks of the commercial HAp (Fig. 3e), but some difference was observed. As for the XRD patterns of the sample calcinated at 923 K (Fig. 3b), the spectrum possessed typical HAp peaks which exactly matched with those of the commercial HAp. This is confirmation of the formation of crystalline phase HAp. As the calcination temperature was increased to 1073 K (Fig. 3c), we can see that the crystallinity of HAp was slightly improved. However, the main phase of HAp coexisted with some other minor impurity phases such as β-TCP and CaO, which resulted from the partial HAp decomposition on silica fiber. When the calcination temperature was further increased up to 1273 K (Fig. 3d), the peaks of HAp became relatively weaker, while the well-defined and sharp peaks corresponding to β-TCP were obviously detected, indicating that the resulting HAp decomposed further at higher temperatures. However, it is worth mentioning that biphasic calcium phosphate ceramics comprising a mixture of HAp and β-TCP are considered better than single phase of HAp or β-TCP for utilization in areas such as bone reconstruction and dental materials.[3,26,27] As evidenced by XRD and TG-DTA measurements, it was shown that the calcination process at 923 K for 5 h would be favorable for coating nano-scale HAp on silica fiber when using CNFs-823 as templates. Energy dispersive spectroscopy (EDS) measurements of the obtained HAp coating on silica fiber showed a Ca/P ratio of 1.78, which provides strong proof of both the presence of HAp and its high purity. EDS results also indicated that Ni atoms (ca. 0.5 wt % as Ni), originating from the prepared catalyst, were still present in obtained HAp coating samples. In addition, elemental analysis did not detect the presence of carbon for the obtained HAp coating on silica fiber, indicating the complete removal of CNFs-823 templates after calcination in air.

Information about the morphology of nano-scale HAp coating on silica fiber obtained at different calcination temperatures for 5 h can be derived from the FE-SEM images (Fig. 4). Figures 4a and 4b correspond to the FE-SEM images of the obtained HAp coating calcinated at 923 K for 5 h. Clearly, HAp coating in this process possessed a uniform and ultrafine microstructure. From the FE-SEM images of HAp coating calcinated at 1073 K for 5 h (Figs. 4c and 4d), we can observe that the morphology of HAp was almost unchanged and the coating of HAp was also uniform. In the case of HAp coating on calcinated at 1273 K for 5 h (Figs. 4e and 4f), the obviously different morphology and crystallite size were observed. The above FE-SEM images suggest that the morphology and crystallite size of nano-scale HAp could be controlled by changing the calcination temperature.

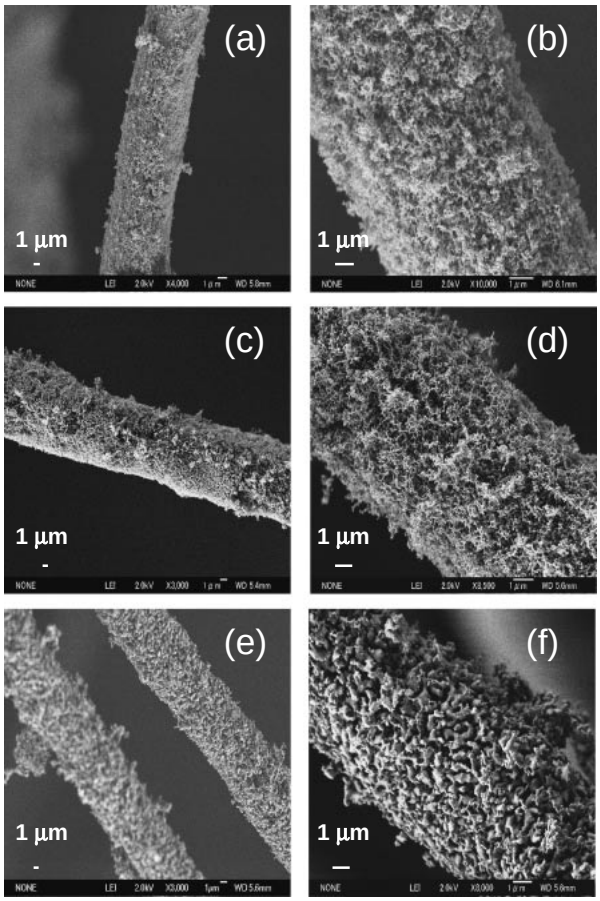

Fig. 4. FE-SEM images of nano-scale HAp coating on silica fiber using CNFs-823 as templates at different calcination temperatures for 5 h. (a) 923 K (low magnification), (b) 923 K (high magnification), (c) 1073 K (low magnification), (d) 1073 K (high magnification), (e) 1273 K (low magnification), and (f) 1273 K (high magnification).

In order to assess the textural properties of the obtained nano-scale HAp coating on silica fiber obtained at different calcination temperatures, the N_2 adsorption–desorption isotherms at 77 K were further determined. The specific surface areas of nano-scale HAp can be calculated as follows: $S_{HAp} = \{(S_{HAp+silica\ fiber} \times W_{HAp+silica\ fiber}) - (S_{silica\ fiber} \times W_{silica\ fiber})\}/W_{HAp}$, where S_{HAp} is the specific surface areas of HAp, $S_{HAp+silica\ fiber}$ is the specific surface area of HAp plus silica fiber, W_{HAp} is the weight of HAp and $W_{HAp+silica\ fiber}$ is the total weight of the obtained HAp plus silica fiber. In addition, the corresponding average crystallite size of each sample was estimated by Scherrer equation. It was shown that the specific surface areas of the obtained samples calcinated at 923, 1073, and 1273 K were 61, 29, and 10 $m^2\ g^{-1}$, respectively. And the corresponding average crystallite sizes were 25, 28, and 69 nm, respectively. Clearly, the specific surface areas of the obtained nano-scale HAp remarkably decreased with the increase of calcination temperature. On the contrary, the corresponding average crystallite size increased with the calcination temperature.

Influence of Different Kinds of CNF Templates on HAp Coating. Since the CNFs synthesized at different tempera-

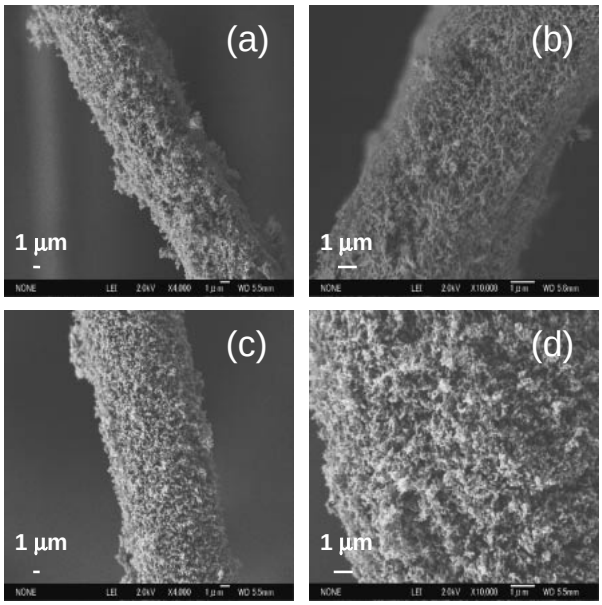

Fig. 5. FE-SEM images of nano-scale HAp coating on silica fiber using different kinds of CNFs as templates calcinated at 923 K for 5 h. (a, b) CNFs-773, (c, d) CNFs-873.

tures possess similar morphologies, except for the remarkable yield difference, layer thickness difference, and diameter difference, it is very interesting to determine how these different CNFs can affect the subsequent coating. Figure 5 shows the FE-SEM images of HAp coating calcinated at 923 K for 5 h using CNFs-773 and CNFs-873 as templates. It is important to note that both templates can also fabricate nano-scale HAp on silica fiber. HAp coating in these two cases possessed morphologies similar to those obtained by using CNFs-823 templates. It was found that average HAp layer thicknesses were ca. 2 and 4 μm when using CNFs-773 and CNFs-873 as templates, respectively. And the corresponding amount of coated HAp was 33% and 78% for each case. Apparently, HAp quantity can be controlled by the amount of CNFs (Table 1).

HAp coating on silica fiber using CNFs-773 and CNFs-873 templates was further characterized by XRD measurements and is presented in Fig. S7 (Supporting Information). It should be noted that the XRD patterns of all samples show diffraction peaks consistent with the commercial HAp, and the average crystallite size of resulting HAp calculated by Scherrer equation was 22 and 31 nm. In addition, the specific surface areas of the resulting HAp were 58 $m^2 g^{-1}$ when using CNFs-773 as templates and 53 $m^2 g^{-1}$ when using CNFs-873 as templates. These results indicate the coating of nano-scale HAp on silica fiber.

Conclusion

We report the first successful coating of nano-scale HAp on macroscopic silica fiber by using CNFs as templates and $Ca(NO_3)_2$–H_3PO_4–methanol as precursor mixtures. CNFs are inert, low-cost, and widely available materials, whose structure can be easily controlled by tuning experimental conditions. XRD, FE-SEM, and cross-sectional TEM experimental results confirmed that CNFs can act as effective templates for mass and uniform nano-scale HAp coating. It was found that heat-treatment at 923 K for 5 h is suitable for the complete removal of the CNFs templates and the crystallization of the resulting nano-scale HAp. It is worthwhile to emphasize that the average layer thickness of HAp was determined by the layer thickness of CNFs. As a result, the properties of HAp could be reliably controlled through the selection of different kinds of CNFs templates. Moreover, this simple and promising template method can be readily extended to the synthesis of a variety of nano-scale materials with controllable morphologies, crystallite size, and yield.

We are grateful for financial support in the form of Grant-in-Aid of Scientific Research (B. No. 18360383). We also acknowledge Mr. Y. Nakasaka for Raman measurements and Dr. F. Wang for TPO measurements.

Supporting Information

TG curves of (a) CNFs-773, (b) CNFs-823 K, and (c) CNFs-873 (Fig. S1), XRD patterns of (a) pure silica fiber, (b) CNFs-773, (c) CNFs-823 K, and (d) CNFs-873 (Fig. S2), Raman spectra of (a) CNFs-773, (b) CNFs-823 K, and (c) CNFs-873 (Fig. S3), Cross-sectional TEM images of HAp coating on silica fiber using CNFs-823 as templates (Fig. S4), TG-DTA curves of Ca–P precursor solution penetrated CNFs-823 templates before calcination with a Ca/P ratio of 1.67 (Fig. S5), TPO profile of HAp coating on CNFs-823 templates (Fig. S6), and XRD patterns of (a) pure silica fiber, (b) HAp coating on silica fiber with CNFs-773 templates, (c) HAp coating on silica fiber using CNFs-823 as templates, (d) HAp coating on silica fiber using CNFs-873 as templates, and (e) commercial HAp. (Fig. S7). This material is available free of charge on the web at http://www.csj.jp/journals/bcsj/.

References

1 E. S. Ahn, N. J. Gleason, A. Nakahira, J. Y. Ying, *Nano Lett.* **2001**, *1*, 149.
2 W. H. Yan, K. Zhang, C. F. Blandford, L. F. Francis, A. Stein, *Chem. Mater.* **2001**, *13*, 1374.
3 B. J. Melde, A. Stein, *Chem. Mater.* **2002**, *14*, 3326.
4 Y. Chen, Y. Q. Zhang, T. H. Zhang, C. H. Gan, C. Y. Zheng, G. Yu, *Carbon* **2006**, *44*, 37.
5 E. Mavropoulos, A. M. Rossi, A. M. Costa, C. A. C. Perez, J. C. Moreira, M. Saldanha, *Environ. Sci. Technol.* **2002**, *36*, 1625.
6 K. Mori, K. Yamaguchi, T. Hara, T. Mizugaki, K. Ebitani, K. Kaneda, *J. Am. Chem. Soc.* **2002**, *124*, 11572.
7 T. Hara, K. Mori, T. Mizugaki, K. Ebitani, K. Kaneda, *Tetrahedron Lett.* **2003**, *44*, 6207.
8 T. Matsumoto, M. Okazaki, M. Inoue, S. Yamaguchi, T. Kusunose, T. Toyonaga, Y. Hamada, J. Takahashi, *Biomaterials* **2004**, *25*, 3807.
9 E. Fujii, M. Ohkubo, K. Tsuru, S. Hayakawa, A. Osaka, K. Kawabata, C. Bonhomme, F. Babonneau, *Acta Biomater.* **2006**, *2*, 69.
10 M. Srinivasan, C. Ferraris, T. White, *Environ. Sci. Technol.* **2006**, *40*, 7054.
11 C. L. Kibby, W. K. Hall, *J. Catal.* **1973**, *31*, 65.
12 T. Tsuchida, S. Sakuma, T. Takeguchi, W. Ueda, *Ind. Eng. Chem. Res.* **2006**, *45*, 8634.
13 I. Zhitomirsky, *Mater. Lett.* **2000**, *42*, 262.
14 C. Kealley, M. Elcombe, A. Riessen, B. Ben-Nissan, *Physica B* **2006**, *385–386*, 496.

15 T. Akasaka, F. Watari, Y. Sato, K. Tohji, *Mater. Sci. Eng., C* **2006**, *26*, 675.
16 J. L. Sui, M. S. Li, Y. P. Lü, L. W. Yin, Y. J. Song, *Surf. Coat. Technol.* **2004**, *176*, 188.
17 T. Furuzono, T. Taguchi, A. Kishida, M. Akashi, Y. Tamada, *J. Biomed. Mater. Res.* **2000**, *50*, 344.
18 H. Ogihara, M. Sadakane, Y. Nodasaka, W. Ueda, *Chem. Mater.* **2006**, *18*, 4981.
19 H. Ogihara, M. Sadakane, Y. Nodasaka, W. Ueda, *Chem. Lett.* **2007**, *36*, 258.
20 K. P. De Jong, J. W. Geus, *Catal. Rev. Sci. Eng.* **2000**, *42*, 481.
21 H. Ogihara, S. Takenaka, I. Yamanaka, K. Otsuka, *Carbon* **2004**, *42*, 1609.
22 H. Ogihara, M. Sadakane, Q. Wu, Y. Nodasaka, W. Ueda, *Chem. Commun.* **2007**, 4047.
23 S. Takenaka, S. Kobayashi, H. Ogihara, K. Otsuka, *J. Catal.* **2003**, *217*, 79.
24 K. Haberko, M. M. Bucko, J. Brzezinska-Miecznik, M. Haberko, W. Mozgawa, T. Panz, A. Pyda, J. Zarebski, *J. Eur. Ceram. Soc.* **2006**, *26*, 537.
25 M. Aizawa, H. Ueno, K. Itatani, I. Okada, *J. Eur. Ceram. Soc.* **2006**, *26*, 501.
26 S. Kannan, J. M. F. Ferreira, *Chem. Mater.* **2006**, *18*, 198.
27 S. Madhavi, C. Ferraris, T. J. White, *J. Solid State Chem.* **2005**, *178*, 2838.